Research Square

Preprints are preliminary reports that have not undergone peer review.
They should not be considered conclusive, used to inform clinical practice,
or referenced by the media as validated information.

Comparative Evaluation of Multicellular Tumor Spheroid Fabrication Platforms for Reliable Drug Screening

Sunghan Lee
Dongguk University
Jaehun Lee
Dongguk University
Min Park
Hallym University
Jiseok Lim
Yeungnam University
Bongseop Kwak
bskwak@dongguk.ac.kr

Dongguk University

Research Article

Keywords: Multicellular tumor spheroids (MTS), Fabrication platform, Drug screening, Dynamic states

Posted Date: July 1st, 2026

DOI: https://doi.org/10.21203/rs.3.rs-9933309/v1

License: This work is licensed under a Creative Commons Attribution 4.0 International License.
Read Full License

Additional Declarations: No competing interests reported.

Version of Record: A version of this preprint was published at Journal of Biological Engineering on August 21st, 2026. See the published version at https://doi.org/10.1186/s13036-026-00750-w.

Abstract

Multicellular tumor spheroids (MTS) are widely used three-dimensional tumor models in various biomedical fields. Despite the increasing use of MTS, systematic comparisons providing practical information for selecting fabrication platforms according to experimental objectives remain limited. In this study, four widely used MTS fabrication platforms (U-bottom, UB; ultra-low attachment, ULA; hanging drop, HD; and droplet microfluidics, DM) were compared in terms of fabrication performance, structural characteristics, and their potential influence on drug screening. Among the platforms, ULA showed the highest fabrication rate, while HD exhibited relatively high size uniformity. In contrast, DM demonstrated balanced performance in both fabrication rate and size uniformity. Structural characteristics of MTS, including morphology and compactness, also varied depending on the fabrication platform. Although these structural differences did not lead to significant differences in drug responses under static states, clear differences in structural stability were observed under dynamic states. MTS with lower compactness exhibited pronounced morphological deformation and size changes. These findings demonstrate that the choice of MTS fabrication platform can influence not only fabrication efficiency but also the structural properties of MTS and endpoint drug response readouts. This study provides practical information for considering fabrication platform-dependent effects in MTS-based drug screening studies.

1. Introduction

Multicellular tumor spheroids (MTS) have emerged as an important three-dimensional tumor model and are widely utilized across diverse biomedical fields, including drug discovery and screening,[1] tumor microenvironment research,[2] integration with organ-on-a-chip systems,[3] and personalized medicine.[4] Despite this expanding use, practical criteria for selecting appropriate fabrication platforms according to specific experimental objectives remain insufficiently established. For example, when cell availability is limited, platforms capable of fabricating MTS from minimal cell input are preferred. In contrast, large-scale drug screening studies benefit from platforms capable of rapid and high-throughput MTS fabrication. Moreover, studies requiring MTS within a specific size range demand platforms capable of precise size control, as MTS size directly influences oxygen and nutrient diffusion, hypoxic core formation, and drug penetration.[5–7] Therefore, objective comparison of available platforms is essential for selecting appropriate fabrication methods according to specific research purposes.

In addition, several potential hidden variables that may significantly influence MTS-based experimental outcomes are often insufficiently considered. Among these variables, the fabrication method is particularly important because it directly determines the environment in which MTS is formed.[8] Various platforms, including U-bottom (UB),[9] ultra-low attachment (ULA),[10, 11] hanging drop (HD),[11, 12] and droplet microfluidics (DM),[13, 14] are widely used for MTS fabrication. These platforms provide distinct culture conditions, such as differences in medium volume, available space for cell movement, and static or dynamic culture environments, which may influence the structural and biological characteristics of the resulting MTS. Indeed, even when the same cell type is used, MTS size and morphology can vary

depending on the fabrication method.[15] Such differences may ultimately introduce bias in drug screening.

In this study, we compared the performance of widely used MTS fabrication platforms in terms of productivity, size uniformity, and MTS quality. Furthermore, MTS fabricated from each platform were subjected to drug treatment to evaluate how structural differences arising from fabrication platforms influence drug response outcomes. Through this approach, we demonstrate that the choice of fabrication platform can affect not only MTS formation but also the interpretation of drug screening, as conceptually shown in Fig. 1.

2. Materials and Methods

2.1 Cell preparation and MTS fabrication

The BT-474 human breast cancer cell line (official name: BT-474; RRID: CVCL_0179) was obtained from the Korea Cell Line Bank (Seoul, Republic of Korea), and used for MTS fabrication. BT474 was maintained using DMEM-high glucose (11965092, Gibco™, NY, USA) with 10% fetal bovine serum (FBS, Gibco™, CA, USA) and 1% penicillin/streptomycin (15140122, Gibco™, CA, USA). Subculture was conducted every three days or reaching 80% confluency.

MTS were fabricated using four platforms: UB (SpheroFilm™, INCYTO, Chungcheongnam-do, Republic of Korea), ULA (CLS3474, Corning, MA, USA), HD (331296, SPL life sciences, Gyeonggi-do, Republic of Korea), and DM (MediSphere Inc., Gyeongsangbuk-do, Republic of Korea). To fabricate MTS with a diameter of 300 μm, cells were diluted in different concentrations for each platform, and we followed each manufacturer's protocol. Briefly, UB was activated with absolute ethanol, 1× DPBS (14190144, Gibco™, MD, USA), and culture media. 7 ml of cell-suspended media was then seeded in UB at 0.5×10^6 cells ml^{-1}. ULA has conventional 96 wells coated with low-cell attachment materials, and 5×10^4 cells were seeded at each well. HD is a plate format, which has 96 holes and can generate 96 drops. 30 μl of 10^5 cells ml^{-1} was dispensed into 96 holes, resulting in cell-suspended drops. DM is a PDMS-based chip that is fabricated from a 3D-printed master mold and consists of a cell-suspended media channel, oil channel, and outlet. The detailed design is provided in Figure S1. 3.0×10^6 cells ml^{-1} of cell-suspended media and 5% surfactant (FluoSurf-C™, Emulseo, France) HFE-7500 oil (3M™, MN, USA) was injected to cell-suspended media and oil channel with 60 μl min^{-1}, and 150 μl min^{-1}, respectively. To fabricate heterogeneously sized MTS using DM, cell concentration was prepared as 0.75, 2.0, 3.0, 7.0, and 10.0 x 10^6 cells ml^{-1} for diameters of 100, 200, 300, 400, and 500 μm, respectively. All MTS fabrication from each platform was achieved by culturing in a cell incubator for 72 hours. The fabrication time and yield were measured in triplicate by three researchers, each with more than three years of experience in the field. The detailed quantitative comparison method is provided in Supporting Information.

2.2 MTS drug screening

MTS fabricated from each platform were individually transferred to ULA plate (3474, CORNING Inc., ME, USA) for drug screening. MTS were incubated with either none or 1 μM doxorubicin in a cell incubator for 24 hours. We analyzed the remission effect using ImageJ software (National Institutes of Health, Bethesda, MD, USA) by comparing the sizes of MTS before drug treatment and after 24 hours. Cell viability within MTS was analyzed through 2,3-bis-(2-methoxy-4-nitro-5-sulfophenyl)2H-tetrazolium-5-carboxanilide (XTT) colorimetric assay (CyQUANT™ XTT Cell Viability assay, X12223, Invitrogen™, OR, USA) and 4',6-diamidino-2-phenylindole (DAPI, Hoechst 33342, 62249, Thermo Scientific™, MA, USA) / propidium iodide (PI, P4864, Sigma-aldrich, MO, USA) staining. After the drug treatment for 24 hours, XTT assay was conducted according to the manufacturer's protocol. In addition, to confirm cell death caused by necrotic core or drug, viability was measured using DAPI/PI solution at a ratio of 1:500 for 2 hours.

For agitation experiments, MTS were transferred to ULA 96-well plates and cultured in a shaking incubator at 37°C and 96 RPM for 24 h. The applied rotation speed was determined to physiologically mimic capillary blood flow, using Eq. (1).

$$\text{Rotation speed } (rpm) = \frac{Blood\ flow\ velocity\ (mm/min)}{Well\ perimeter\ (mm)} \times 60$$

1

In this equation, the blood flow velocity was set to 36 mm min^{-1}, reflecting the average flow velocity in capillaries as reported previously.[16] The well perimeter was calculated as 22.46 mm based on the radius (3.57 mm) of a standard 96-well plate. Substituting these values yielded 96.1 RPM, which was adopted as the experimental condition. This calculation ensured that MTS were exposed to dynamic culture conditions comparable to physiological capillary shear environments.

2.3 Morphological and compactness analysis

Circularity and convexity of MTS were analyzed by the following Equations (2, 3).

$$Circularity = \frac{4 * \pi\ * Area}{Convex\ Perimeter^2}$$

2

,

$$Convexity = \frac{Convex\ Perimeter}{Perimeter}$$

3

.

Circularity is a quantitative indicator that measures the degree to which MTS resembles a perfect circle, with values ranging from 0 to 1. Higher values indicate a shape closer to a perfect circle. *Area* quantifies the number of pixels occupied by the MTS, and *Convex Perimeter* represents the perimeter measured using the convex mask. Convexity measures how much a shape deviates from being convex or concave. Convexity, ranging from 0 to 1, indicates the smoothness of the MTS surface, with values closer to 1 representing a smoother surface. All MTS images were captured at the same exposure time (10 ms) using a single brightfield microscope for the conversion of brightfield images to a heatmap. MTS with diameters close to the target size of 300 μm were selected as much as possible to reduce size-related effects on brightness and transmittance. The heatmap imaging for transmittance analysis was conducted using the "Look Up Tables" (LUT) function in the ImageJ software. The LUT represents dark pixels as red and bright pixels as blue. For void area analysis, MTS were sectioned at 4-μm intervals, and one representative section containing the largest cross-sectional diameter was selected from each MTS for quantification. A total of 4–5 MTSs per platform were analyzed.

2.4 Scanning electron microscope (SEM)

For preparation SEM images, we removed the supernatant from the tube containing the MTSs and incubated with 4% formaldehyde solution (Tech & Innovation, Gangwon-do, Republic of Korea) at room temperature for an hour, followed by washing three times with 1x DPBS (Gibco, MA, USA) and incubating in 1% osmium tetroxide solution (75632, Sigma-aldrich, MO, USA) for 30 minutes at room temperature. Then, the fixed MTSs were dehydrated in 30%, 50%, 70%, 80%, 90%, and 100% ethanol (E7023, Sigma-aldrich, MO, USA) for 10 minutes each. The dehydrated samples were placed on a silicon wafer, allowing them to air dry to remove the solution. The MTSs were completely dried using 100% HMDS (440191, Sigma-aldrich, MO, USA). After the drying, platinum coating was performed at 10 nm thickness. SEM images were obtained using a Gemini SEM 560 (Zeiss, Germany)

2.5 H&E Staining

MTS were fixed in 4% paraformaldehyde, dehydrated through a graded ethanol series, and subsequently embedded in paraffin. The paraffin-embedded MTS were then sectioned to a thickness of 4 μm and placed onto polysine slides. Following this, the sections were stained with hematoxylin and eosin and imaged. The obtained images were converted to black and white using the “Threshold” function in ImageJ to measure the empty area.

2.6 Statistical Analysis

Statistical analyses were performed using Origin 2024 software. All data are presented as mean ± standard deviation. For comparisons between two groups, Student’s t-test was used. For analyses involving multiple groups or two independent factors, one-way or two-way analysis of variance (ANOVA) was performed, as appropriate. All statistical tests were conducted with an alpha level of 0.05. Statistical significance was defined as $p < 0.05$ (*), $p < 0.01$ (**), and $p < 0.001$ (***).

3. Results and discussion

3.1 Platforms for MTS fabrication

The detailed schematics and the corresponding optical images of the four platforms used in this study are shown in Fig. 2(a,b). In brief, UB involves seeding cells onto a U-curved structure at the bottom, where MTS are formed on the bottom surface due to gravity. ULA induces cells to self-assemble with neighboring cells into MTS instead of adhering to the bottom surface. HD induces cells to accumulate at the tip of a drop due to gravity, allowing them to form MTS. DM utilizes a microfluidic system to encapsulate cells within droplets, allowing for the formation of MTS. Figure 2(c,d) shows microscopic images of MTS fabricated with a target diameter of 300 μm on each platform. This diameter is considered to be suitable for drug screening.[14] In UB, multiple MTS were sometimes formed in each well, and in ULA, multiple MTS with heterogeneous sizes and morphologies were formed in each well. In contrast, a single MTS was always formed within each drop in HD and DM. Therefore, HD and DM are more advantageous for achieving the targeted size compared to UB and ULA.

3.2 Fabrication performance

Figure 3(a,b) shows MTS collected from each platform and transferred to a culture dish. The collected MTS exhibit consistent size and morphology with their respective platforms before collection, as shown in Figs. 1(d) and 2(b), suggesting negligible damage or loss to MTS during the collection process. The productivity of each platform, evaluated by fabrication rate (MTSs per second) and yield (each per batch), is shown in Fig. 3(c). The UB exhibited relatively poor performance in both fabrication rate and yield, whereas the ULA demonstrated the highest fabrication rate while maintaining a high yield. In contrast, the HD platform showed the lowest values for both metrics, and DM showed relatively high fabrication rate and yield. In terms of productivity, the ULA platform showed the highest performance, followed by DM, UB, and HD. It should be noted, however, that the fabrication yield of ULA and HD can be further increased by using higher-well-density plates, such as 384- or 1536-well formats. However, the fabrication rate is largely governed by the dispensing and handling process, since each well requires loading of the cell-suspended medium. Therefore, the well-plate format and operation mode should be considered when interpreting the throughput of well plate-based MTS fabrication platforms. Figure 3(d) shows the diameter of the MTS fabricated with a target diameter of 300 μm on each platform. The diameters of MTS fabricated from UB, ULA, HD, and DM were 206.5 ± 73.7 μm (N = 50), 187.2 ± 79.5 μm (N = 50), 316.8 ± 18.0 μm (N = 50), and 291.2 ± 7.9 μm (N = 50), respectively. These results indicate that each platform exhibits distinct characteristics in terms of productivity and size uniformity. ULA are advantageous for high-throughput MTS fabrication, whereas HD provides relatively high size uniformity. DM shows a balanced performance in terms of both productivity and size control.

3.3 Quality of MTS

The quality of MTS was evaluated based on compactness and morphology. Compactness reflects internal cellular packing, whereas morphology, assessed by circularity and convexity, describes external shape integrity. Stronger cell-cell adhesion can promote denser cellular packing by reducing internal void

spaces, thereby increasing compactness. Such cell rearrangement and compaction can be interpreted in the context of the differential adhesion hypothesis (DAH), which proposes that cell aggregates self-organize through cell-cell adhesion and tissue surface tension to minimize adhesive free energy.[17, 18] Therefore, collective cellular adhesion or cohesion may contribute to both internal compaction and the formation of a more rounded and smoother external morphology. Moreover, drug-response readouts in MTS-based assays can be influenced by compactness and morphology; thus, both parameters were assessed to evaluate platform-dependent MTS quality.[7] Fig. 4(a) shows brightfield microscopic images of MTS with a target diameter of 300 μm. As MTS become denser and more compact, microscopic images appear darker due to reduced intercellular space and a tighter internal structure.[15, 19] Fig. 4(b) presents transmittance-based heatmap images, where red indicates regions of highest compactness. This visualization provides a clearer differentiation of compactness among fabrication platforms, with DM producing the most compact MTS, followed by ULA, UB, and HD. To confirm compactness more quantitatively and intuitively, we analyzed the void areas in MTS cross-sections from four to five MTS samples per platform (N = 4–5), as shown in Figs. 4(c,e). Consistent with the heatmap data, MTS from DM exhibited the least void space.

Figure 4(d) shows SEM images that highlight a correlation between MTS compactness and morphology. MTS from DM, which had the highest compactness, showed a smooth surface, indicating tight cell-cell adhesion. In contrast, MTS from UB exhibited a rough surface with irregularities, and MTS from HD showed visible cell-cell boundaries, indicating weaker intercellular adhesion. Figures 4(f) and 4(g) show circularity and convexity, respectively, based on six MTS samples per platform (N = 6). Circularity was highest for DM at 0.90 ± 0.02, followed by ULA (0.86 ± 0.06), HD (0.86 ± 0.04), and UB (0.82 ± 0.10). Convexity followed a similar trend, with values of DM at (0.92 ± 0.02), ULA (0.90 ± 0.04), HD (0.89 ± 0.03), and UB (0.86 ± 0.08). These results suggest that the structural compactness and morphological characteristics of MTS may vary depending on the fabrication platform. Notably, the overall trends of compactness and morphology were generally consistent across the fabrication platforms. DM-derived MTS exhibited both the highest compactness and the most stable morphology, followed by ULA, whereas UB and HD showed relatively lower structural quality. This trend suggests that denser internal packing may be associated with smoother and more uniform external morphology, supporting the use of both parameters as complementary indicators of MTS structural quality. The expression of E-cadherin, a representative cell-cell adhesion molecule involved in MTS compaction, was additionally investigated.[7] However, as shown in Figure S2, E-cadherin expression did not correlate with the compactness trend determined by transmittance heatmap and void area analysis. This discrepancy suggests that MTS compactness is not solely governed by E-cadherin-mediated cell adhesion, but may also be influenced by other biophysical and environmental factors, such as molecular interaction probability, nutrient stress, and fluid dynamics during MTS formation.

3.4 Drug evaluation under static states

The prior sections confirmed that MTS exhibit different compactness and morphological characteristics depending on the fabrication platform. To determine whether these structural differences could

influence drug screening outcomes, drug effects were evaluated using MTS size change and cell viability, which are commonly used readouts for assessing growth inhibition and cytotoxicity in MTS-based drug screening.[8] As shown in Fig. 5(a), MTS from all platforms exhibited an overall increase in size over 24 hours without the drug (W/O drug), whereas this growth was suppressed with the drug (W/ drug), suggesting that the drug affects changes in MTS size. Figure 5(b) shown the comparison of MTS sizes after 24 hours without the drug and with the drug. MTS from UB, HD, and DM increased to 119.4 ± 3.1 %,115.1 ± 3.7 %,and 116.0 ± 1.9 %,respectively, without the drug, but only to 106.9 ± 2.3 %,106.4 ± 4.1 %,and 106.9 ± 3.0 % ith the drug (N = 5). In contrast, the MTS from ULA showed a relatively smaller increase (107.2 ± 7.6 %)without the drug and even a slight decrease (93.3 ± 6.9 %)with the drug. This difference is likely attributable to the smaller MTS size in the ULA platform, as ULA failed to fabricate MTS with the target diameter (300 μm), as shown in Fig. 2(d). Considering that MTS size can influence drug diffusion and penetration,[7] the relatively higher drug sensitivity observed in ULA-derived MTS is likely associated with their smaller size. Consistently, Figures S3 and S4 demonstrate that MTS size influences morphological characteristics and drug responsiveness, with larger MTS exhibiting greater resistance to drug treatment. To further assess the drug effect, cell viability was also evaluated. Figure 5(c) shows that cell viability within all MTS was nearly 100% without the drug. With the drug, cell viability within MTS from UB, ULA, HD, and DM was 91.0 ± 3.4%, 90.8 ± 1.5%, 88.8 ± 2.3%, and 90.8 ± 3.8%, respectively (N = 5). Overall, platform-dependent differences in MTS quality did not lead to clear differences in drug response under static states. This suggests that fabrication-dependent bias may be less pronounced in static drug evaluation. However, the relatively higher drug sensitivity observed in ULA-derived MTS indicates that insufficient size control can still affect the interpretation of drug responses.

3.5 Drug evaluation under dynamic states

While no difference in the drug effect on MTS among the platforms was observed under static states, recent studies have emphasized that dynamic environments providing fluid flow and shear stress may enhance physiological relevance and are therefore important for evaluating drug responses.[3, 20–22] Accordingly, the drug effect was validated under dynamic states with fluid agitation, as shown in Fig. 6(a). Except for MTS from DM, all others exhibited pronounced morphological deformation under dynamic states regardless of drug presence, indicating a loss of structural stability, as shown in Fig. 6(b,c). MTS from DM maintained relatively high circularity and convexity without drug (0.84 ± 0.05 and 0.86 ± 0.06, respectively). In contrast, MTS from HD, ULA, and UB showed markedly lower circularity (0.54 ± 0.21, 0.50 ± 0.05, and 0.48 ± 0.05, respectively) and convexity (0.57 ± 0.21, 0.53 ± 0.05, and 0.51 ± 0.05, respectively) without drug, based on six MTS samples per platform (N = 6), as shown in Figs. 5(d,e). Similar trends were observed with drug, indicating substantial morphological deformation under dynamic states. Figure 6(f) shows that the changes in MTS size under dynamic states differed depending on the fabrication platform. Without drug, DM exhibited a size increase of 111.7 ± 3.6%, whereas this increase was suppressed to 102.68 ± 4.6% with drug treatment. In contrast, MTS fabricated using HD, ULA, and UB showed an opposite trend, increasing from 102.9 ± 10.3% to 120.3 ± 6.7%, from 94.6 ± 3.5% to 111.7 ± 7.9%, and from 114.1 ± 3.8% to 123.6 ± 7.2%, respectively. Notably, the size

increase observed in HD, ULA, and UB after drug treatment under dynamic conditions may be attributed to agitation-induced structural loosening rather than true biological growth. These MTS showed lower compactness and greater morphological deformation, suggesting that fluidic shear can alter MTS morphology and cell-cell adhesion, resulting in deformation-related size changes.[23] In contrast, DM-derived MTS maintained structural integrity under the same fluidic conditions, which may have reduced deformation-related size changes. These results are likely associated with the higher compactness of DM-derived MTS, as shown in Fig. 4. Although resistance to fluidic agitation can be influenced by multiple mechanical factors, [24, 25] the compact architecture of DM-derived MTS, characterized by reduced void space and dense cellular packing, may contribute to their resistance against mechanical perturbation under dynamic conditions. Figure 6(g) shows that cell viability under dynamic conditions tended to decrease compared with that under static state across all platforms. Without agitation, the viability of MTS was 95.2 ± 2.5%, 93.7 ± 3.6%, 92.3 ± 6.1%, and 93.5 ± 4.0% for DM, HD, ULA, and UB, respectively (N = 5). Under agitation, viability decreased to 92.1 ± 3.4%, 90.4 ± 2.3%, 80.4 ± 5.2%, and 90.0 ± 2.4%, respectively (N = 5), with the most pronounced reduction observed in ULA-derived MTS. Collectively, these results suggest that the structural stability and compactness of MTS are critical factors when evaluating drug responses under dynamic states. More compact MTS are less susceptible to structural loosening and morphological deformation induced by fluid agitation, thereby enabling more reliable drug response assessment.

3.6 Hypotheses for the variability in MTS across different fabrication processes

As we have observed marked differences in the characteristics of MTS, such as compactness and morphology, depending on the platforms, we note that others have also observed that MTS formed by different methods exhibit variations in size and morphology, but the cause of this phenomenon has yet to be identified.[26] This issue must be explored to improve the reliability and utilization of MTS. We introduce three hypotheses: intercellular distance (D_{IC}), nutrient stress, and fluidic dynamics, all of which are influenced during MTS formation.

First, D_{IC} must be close enough for the molecules required for initial cellular aggregation to actively interact. Initial aggregation through self-assembly is a crucial step because MTS formation sometimes fails if it is not achieved within a certain period (72 hours).[15] In particular, a shorter D_{IC} may increase the opportunity for early cell-cell contact. Since MTS formation involves sequential aggregation and compaction steps, in which E-cadherin-mediated adhesion and cytoskeleton-associated processes have been implicated, enhanced early contact may facilitate subsequent compaction of aggregated cells.[27, 28] D_{IC} closely corresponded to the trend of compactness and morphology of MTS. As shown in Fig. 7(a), D_{IC} was measured as 168 μm for UB, 98 μm for ULA, 134 μm for HD, and 82 μm for DM. According to the results noted in Fig. 4, compactness was highest in the descending order of DM, ULA, UB, and HD, while morphological stability followed the order of DM, ULA, HD, and UB. This suggests that

smaller D_{IC} values promote more active cell-cell, leading to faster initial aggregation and the subsequent formation of MTS with higher compactness and morphological stability.

Second, cells experience nutrient stress because not only is MTS compaction progressing, but also the volume of media available to each cell during MTS formation is limited. Nutrient stress can induce autophagy, which regulates cellular energy balance and supports cell survival under metabolically unfavorable conditions.[29–33] It has been linked to integrin-mediated adhesion, focal adhesion turnover, and cellular adaptation under metabolic or detachment stress.[34] Therefore, nutrient stress-induced autophagic responses may partly contribute to platform-dependent differences in MTS compactness and morphological stability by modulating cellular survival and adhesion-related remodeling. As shown in Fig. 7(b), the volume of medium available to each cell was measured as 2 nl $cell^{-1}$ for UB, 0.42 nl $cell^{-1}$ for ULA, 1 nl $cell^{-1}$ for HD, and 0.23 nl $cell^{-1}$ for DM. MTS formed under lower medium volumes per cell tended to exhibit higher compactness and greater morphological stability. This suggests that limited medium availability may contribute to MTS compaction through nutrient stress-related cellular responses, although excessive nutrient limitation could also negatively affect cell viability depending on culture conditions.

Lastly, Increased cell-cell collisions induced by fluid flow, which can promote tighter cellular aggregation. MTS fabricated using the DM platform exhibited distinctively higher compactness and morphological stability. The presence of surfactant micelles in the oil phase around the droplets in DM triggers Marangoni instability to minimize the overall surface energy of the system.[35–39] This phenomenon induces vortical flows inside the droplet, causing the suspended cells to advect accordingly, as shown in Fig. 7(c). Such dynamic motion resembles the spinner flask method, in which continuous collisions among cells enhance MTS formation, providing an additional effect that promotes compact MTS assembly. In addition, the internal fluidic motion within droplets may expose cells to shear stress. fluid shear stress induces EMT-like responses in cancer cells, including the downregulation of epithelial markers such as E-cadherin.[40, 41] Therefore, the lower E-cadherin expression observed in DM-derived MTS may be partly associated with fluid-induced epithelial-to-mesenchymal transition (EMT)-like changes during droplet-based formation. This may explain the apparent discrepancy that DM-derived MTS exhibited higher compactness despite lower E-cadherin expression.

4. Conclusion

In this study, we analyzed the fabrication performance of four widely used platforms for MTS fabrication (UB, ULA, HD, and DM) and investigated the potential for platform-dependent bias in drug evaluation. ULA exhibited the highest fabrication rate, while HD and DM showed relatively high size uniformity. In particular, the DM platform demonstrated balanced performance in terms of both productivity and size control. In addition, differences were observed in the structural characteristics of MTS depending on the fabrication platform. MTS fabricated using the DM platform exhibited the highest compactness and morphological stability, followed by ULA, UB, and HD. These findings suggest that even when the same cell type is used, the internal structure and morphological characteristics of MTS can vary depending on

the fabrication platform. Such variations in MTS characteristics may potentially lead to platform-dependent bias in drug response evaluation.

Drug evaluation under static states revealed no significant differences in drug responses among platforms despite structural differences in MTS. However, when MTS size is not sufficiently controlled, variability in experimental outcomes arise. In contrast, under dynamic states, clear differences in structural stability were observed among platforms. MTS fabricated using the DM platform maintained their morphological stability, whereas those fabricated by other platforms exhibited morphological deformation. These findings indicate that compactness and structural stability of MTS are important factors when evaluating drug responses under physiologically more relevant dynamic environments. Importantly, the superior structural stability of DM-derived MTS under dynamic conditions should not be interpreted as indicating that they are inherently superior tumor models under all experimental conditions. Rather, these results suggest that fabrication platform-dependent structural integrity can influence endpoint readouts in dynamic MTS-based drug evaluation and should therefore be considered when interpreting drug response results.

In our previous review study, we proposed that MTS size, cell viability, and fabrication methods are major factors that may introduce bias in MTS-based drug screening.[8] While many studies acknowledge that MTS size and cell viability can influence experimental outcomes through mechanisms such as drug resistance and hypoxic core formation, systematic discussions regarding fabrication methods remain limited. This study demonstrates that the choice of MTS fabrication platform affects not only fabrication efficiency but also the structural properties of MTS and the reliability of drug response evaluation. These findings highlight the importance of selecting appropriate fabrication platforms according to experimental objectives in MTS-based drug screening studies. Although this study demonstrated that platform-dependent structural differences can influence endpoint drug response readouts, the direct mechanistic relationship between MTS compactness and biological responses remains to be further investigated. Future studies directly linking structural differences with biological responses will provide a more comprehensive understanding of how fabrication-dependent structural variations affect biological drug responses in MTS-based assays.

Declarations

Funding declaration

This work was supported by the National Research Foundation of Korea (NRF) grant funded by the Korean government (MSIT)(NRF-2021R1A6A1A03039493, NRF-2022R1A2C1009389 and NRF-RS-2025-25425984), and Korea Environment Industry & Technology Institute(KEITI) through Technology Development Project for Safety Management of Household Chemical Products Project, funded by Korea Ministry of Environment (MOE)(RS-2025-02223058).

Ethics and Consent to Participate declarations

Not applicable

Conflict of interests

The authors declare that they have no known competing financial interest or personal relationships that could have appeared to influence the work reported in this paper.

Contributions

Sunghan Lee: Data curation, Investigation, Methodology, Writing - original draft. **Jaehun Lee:** Data curation, Investigation, Methodology, Validation, Visualization. **Min Park:** Resources, Writing - review and editing, Investigation. **Jiseok Lim:** Funding acquisition, Project administration, Resources, Writing - review and editing. **Bongseop Kwak:** Conceptualization, Investigation, Supervision, Visualization, Writing - review and editing.

Data availability

The data supporting the findings of this study can be obtained from the corresponding author upon a reasonable request.

References

1. Friedrich J, Seidel C, Ebner R, Kunz-Schughart LA. Spheroid-based drug screen: considerations and practical approach. Nat Protoc [Internet]. 2009;4:309–24. https://doi.org/10.1038/nprot.2008.226.
2. Shah S, D'Souza GGM. Modeling tumor microenvironment complexity in vitro: spheroids as physiologically relevant tumor models and strategies for their analysis. Cells MDPI. 2025;14:732.
3. Kim Y, Lee J, Lee S, Jung H-I, Kwak B. Anisotropic tumor spheroid remission with binary tumor-microenvironment-on-a-chip. Biosens Bioelectron [Internet]. 2024;243:115787. https://doi.org/https://doi.org/10.1016/j.bios.2023.115787.
4. Raghavan S, Mehta P, Ward MR, Bregenzer ME, Fleck EMA, Tan L, et al. Personalized medicine–based approach to model patterns of chemoresistance and tumor recurrence using ovarian cancer stem cell spheroids. Clin Cancer Res Am Association Cancer Res. 2017;23:6934–45.
5. Singh SK, Abbas S, Saxena AK, Tiwari S, Sharma LK, Tiwari M. Critical role of three-dimensional tumorsphere size on experimental outcome. Biotechniques Taylor Francis. 2020;69:333–8.
6. Zhu S, Yin J, Lu X, Jiang D, Chen R, Cui K, et al. Influence of experimental variables on spheroid attributes. Sci Rep Nat Publishing Group UK Lond. 2025;15:9751.
7. Han SJ, Kwon S, Kim KS. Challenges of applying multicellular tumor spheroids in preclinical phase. Cancer Cell Int [Internet]. 2021;21:152. https://doi.org/10.1186/s12935-021-01853-8.
8. Lee S, Lim J, Kwak B. Factors of bias in spheroid-based drug screening: Fabrication method, spheroid size, and cell viability. Biomed Pharmacotherapy [Internet]. 2025;192:118597. https://doi.org/https://doi.org/10.1016/j.biopha.2025.118597.

9. Jo Y, Choi N, Kim HN, Choi J. Probing characteristics of cancer cells cultured on engineered platforms simulating different microenvironments. Artif Cells Nanomed Biotechnol [Internet] Taylor Francis. 2018;46:1170–9. https://doi.org/10.1080/21691401.2018.1446970.
10. Luo L, Zhang W, Wang J, Zhao M, Shen K, Jia Y, et al. A Novel 3D Culture Model of Human ASCs Reduces Cell Death in Spheroid Cores and Maintains Inner Cell Proliferation Compared With a Nonadherent 3D Culture. Front Cell Dev Biol [Internet]. 2021;9. https://doi.org/10.3389/fcell.2021.737275.
11. Raghavan S, Mehta P, Horst EN, Ward MR, Rowley KR, Mehta G. Comparative analysis of tumor spheroid generation techniques for differential in vitro drug toxicity. Oncotarget United States. 2016;7:16948–61. https://doi.org/10.18632/oncotarget.7659.
12. Tung Y-C, Hsiao AY, Allen SG, Torisawa Y, Ho M, Takayama S. High-throughput 3D spheroid culture and drug testing using a 384 hanging drop array. Analyst [Internet] Royal Soc Chem. 2011;136:473–8. https://doi.org/10.1039/C0AN00609B.
13. Kwak B, Lee Y, Lee J, Lee S, Lim J. Mass fabrication of uniform sized 3D tumor spheroid using high-throughput microfluidic system. J Controlled Release [Internet] Elsevier. 2018;275:201–7. https://doi.org/10.1016/j.jconrel.2018.02.029.
14. Lee J, Kim Y, Lim J, Jung H-I, Castellani G, Piccinini F, et al. Optimization of Tumor Spheroid Preparation and Morphological Analysis for Drug Evaluation. Biochip J [Internet]. 2024. https://doi.org/10.1007/s13206-024-00143-5.
15. Cavo M, Delle Cave D, D'Amone E, Gigli G, Lonardo E, del Mercato LL. A synergic approach to enhance long-term culture and manipulation of MiaPaCa-2 pancreatic cancer spheroids. Sci Rep [Internet]. 2020;10:10192. https://doi.org/10.1038/s41598-020-66908-8.
16. Gould IG, Tsai P, Kleinfeld D, Linninger A. The capillary bed offers the largest hemodynamic resistance to the cortical blood supply. J Cereb Blood Flow Metab United States. 2017;37:52–68. https://doi.org/10.1177/0271678X16671146.
17. Foty RA, Steinberg MS. The differential adhesion hypothesis: a direct evaluation. Dev Biol. 2005;278:255–63. https://doi.org/10.1016/j.ydbio.2004.11.012.
18. Leung BM, Lesher-Perez SC, Matsuoka T, Moraes C, Takayama S. Media additives to promote spheroid circularity and compactness in hanging drop platform. Biomater Sci. 2015;3:336–44. https://doi.org/10.1039/C4BM00319E.
19. Madhavan M, Jaiswal D, Karlberg S, Duggan A, Almarshad HA, Claffey KP, et al. Electron microscopy imaging and mechanical characterization of T47D multicellular tumor spheroids-Older spheroids reduce interstitial space and become stiffer. PLoS One United States. 2023;18:e0286291. https://doi.org/10.1371/journal.pone.0286291.
20. Masiello T, Dhall A, Hemachandra LPM, Tokranova N, Melendez JA, Castracane J. A Dynamic Culture Method to Produce Ovarian Cancer Spheroids under Physiologically-Relevant Shear Stress. Cells. 2018. https://doi.org/10.3390/cells7120277.

21. Zhuang J, Zhang J, Wu M, Zhang Y. A Dynamic 3D Tumor Spheroid Chip Enables More Accurate Nanomedicine Uptake Evaluation. Advanced Science [Internet]. Wiley, Ltd; 2019;6:1901462. https://doi.org/https://doi.org/10.1002/advs.201901462
22. Bourn MD, Batchelor DVB, Ingram N, McLaughlan JR, Coletta PL, Evans SD, et al. High-throughput microfluidics for evaluating microbubble enhanced delivery of cancer therapeutics in spheroid cultures. J Controlled Release [Internet]. 2020;326:13–24. https://doi.org/https://doi.org/10.1016/j.jconrel.2020.06.011.
23. Senrung A, Lalwani S, Janjua D, Tripathi T, Kaur J, Ghuratia N, et al. 3D tumor spheroids: morphological alterations a yardstick to anti-cancer drug response. vitro models. 2023;2:219–48. https://doi.org/10.1007/s44164-023-00059-8.
24. Efremov YM, Zurina IM, Presniakova VS, Kosheleva NV, Butnaru DV, Svistunov AA, et al. Mechanical properties of cell sheets and spheroids: the link between single cells and complex tissues. Biophys Rev. 2021;13:541–61. https://doi.org/10.1007/s12551-021-00821-w.
25. Boot RC, van der Net A, Gogou C, Mehta P, Meijer DH, Koenderink GH, et al. Cell spheroid viscoelasticity is deformation-dependent. Sci Rep. 2024;14:20013. https://doi.org/10.1038/s41598-024-70759-y.
26. Shoval H, Karsch-Bluman A, Brill-Karniely Y, Stern T, Zamir G, Hubert A, et al. Tumor cells and their crosstalk with endothelial cells in 3D spheroids. Sci Rep [Internet]. 2017;7:10428. https://doi.org/10.1038/s41598-017-10699-y.
27. Devanny AJ, Vancura MB, Kaufman LJ. Exploiting differential effects of actomyosin contractility to control cell sorting among breast cancer cells. Mol Biol Cell. 2021;32. https://doi.org/10.1091/mbc.E21-07-0357.
28. Smyrek I, Mathew B, Fischer SC, Lissek SM, Becker S, Stelzer EHK. E-cadherin, actin, microtubules and FAK dominate different spheroid formation phases and important elements of tissue integrity. Biol Open. 2019;8. https://doi.org/10.1242/bio.037051.
29. Jiang P, Gan M, Lin W-L, Yen S-HC. Nutrient deprivation induces α-synuclein aggregation through endoplasmic reticulum stress response and SREBP2 pathway. Front Aging Neurosci Switz. 2014;6:268. https://doi.org/10.3389/fnagi.2014.00268.
30. Aman Y, Schmauck-Medina T, Hansen M, Morimoto RI, Simon AK, Bjedov I, et al. Autophagy in healthy aging and disease. Nat Aging [Internet]. 2021;1:634–50. https://doi.org/10.1038/s43587-021-00098-4.
31. Glick D, Barth S, Macleod KF. Autophagy: cellular and molecular mechanisms. J Pathol Engl. 2010;221:3–12. https://doi.org/10.1002/path.2697.
32. Li X, Zhou Y, Li Y, Yang L, Ma Y, Peng X, et al. Autophagy: A novel mechanism of chemoresistance in cancers. Biomed Pharmacotherapy [Internet]. 2019;119:109415. https://doi.org/https://doi.org/10.1016/j.biopha.2019.109415.
33. Chang H, Zou Z. Targeting autophagy to overcome drug resistance: further developments. J Hematol Oncol [Internet]. 2020;13:159. https://doi.org/10.1186/s13045-020-01000-2.

34. Vlahakis A, Debnath J. The Interconnections between Autophagy and Integrin-Mediated Cell Adhesion. J Mol Biol. 2017;429:515–30. https://doi.org/10.1016/j.jmb.2016.11.027.
35. Jia F, Peng X, Wang J, Wang T, Sun K. Marangoni-driven spreading of a droplet on a miscible thin liquid layer. J Colloid Interface Sci [Internet]. 2024;658:617–26. https://doi.org/https://doi.org/10.1016/j.jcis.2023.12.092.
36. Nikkhah A, Shin S. Marangoni flows triggered by cationic-anionic surfactant complexation. J Colloid Interface Sci Elsevier. 2024;676:168–76.
37. Michelin S. Self-propulsion of chemically active droplets. Annu Rev Fluid Mech Annual Reviews. 2023;55:77–101.
38. Kalli M, Pico P, Chagot L, Kahouadji L, Shin S, Chergui J, et al. Effect of surfactants during drop formation in a microfluidic channel: a combined experimental and computational fluid dynamics approach. J Fluid Mech. 2023;961:A15. https://doi.org/10.1017/jfm.2023.213.
39. Baret J-C. Surfactants in droplet-based microfluidics. Lab Chip. 2012;12:422–33. https://doi.org/10.1039/C1LC20582J.
40. Fuh KF, Shepherd RD, Withell JS, Kooistra BK, Rinker KD. Fluid flow exposure promotes epithelial-to-mesenchymal transition and adhesion of breast cancer cells to endothelial cells. Breast Cancer Res. 2021;23:97. https://doi.org/10.1186/s13058-021-01473-0.
41. Araki K, Shimura T, Suzuki H, Tsutsumi S, Wada W, Yajima T, et al. E/N-cadherin switch mediates cancer progression via TGF-β-induced epithelial-to-mesenchymal transition in extrahepatic cholangiocarcinoma. Br J Cancer. 2011;105:1885–93. https://doi.org/10.1038/bjc.2011.452.

Figures

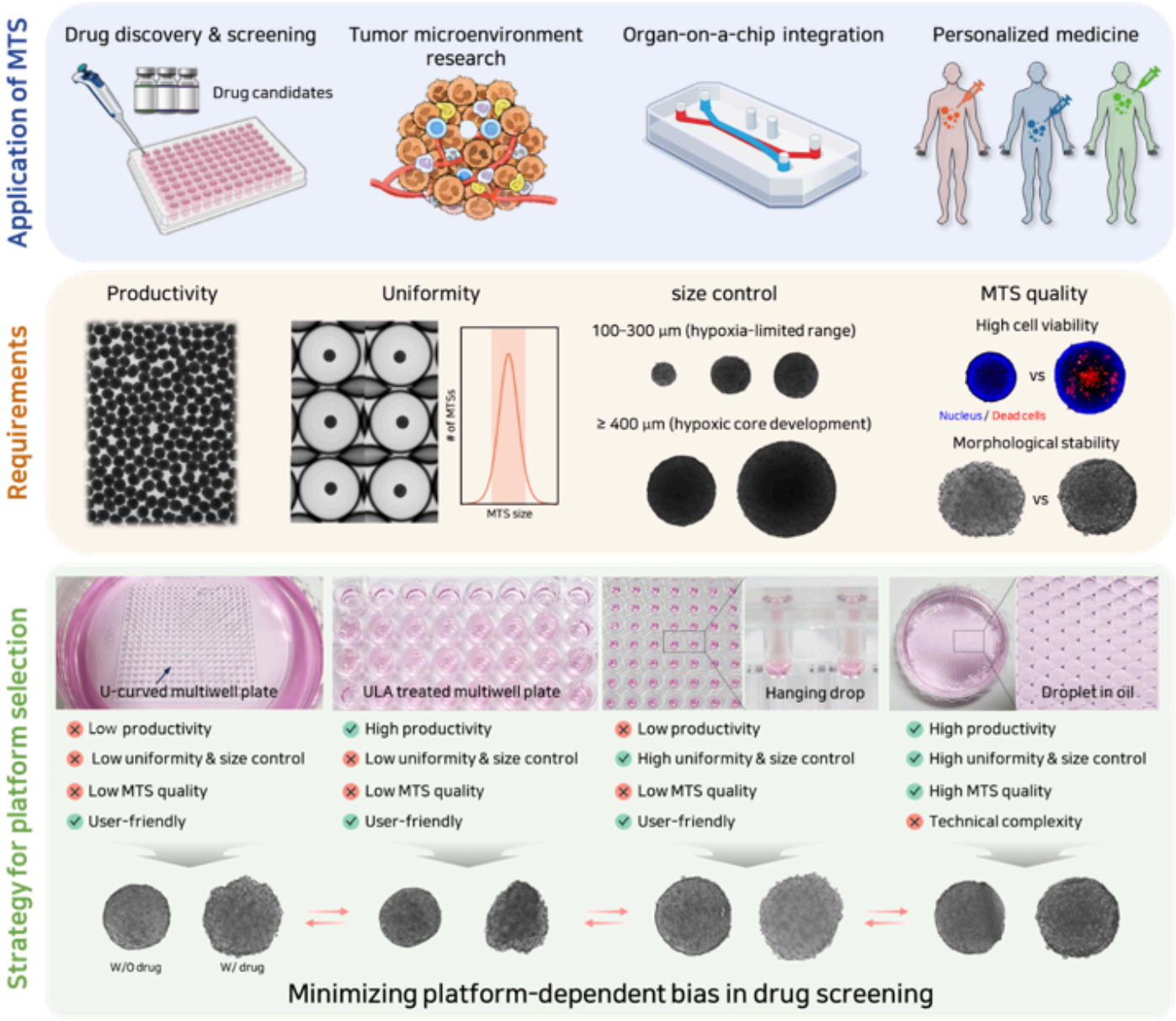


Figure 1

Overview of this study: applications of MTS, key experimental requirements arising from these applications, and a conceptual strategy for selecting fabrication platforms to minimize platform-dependent bias in MTS-based drug screening.

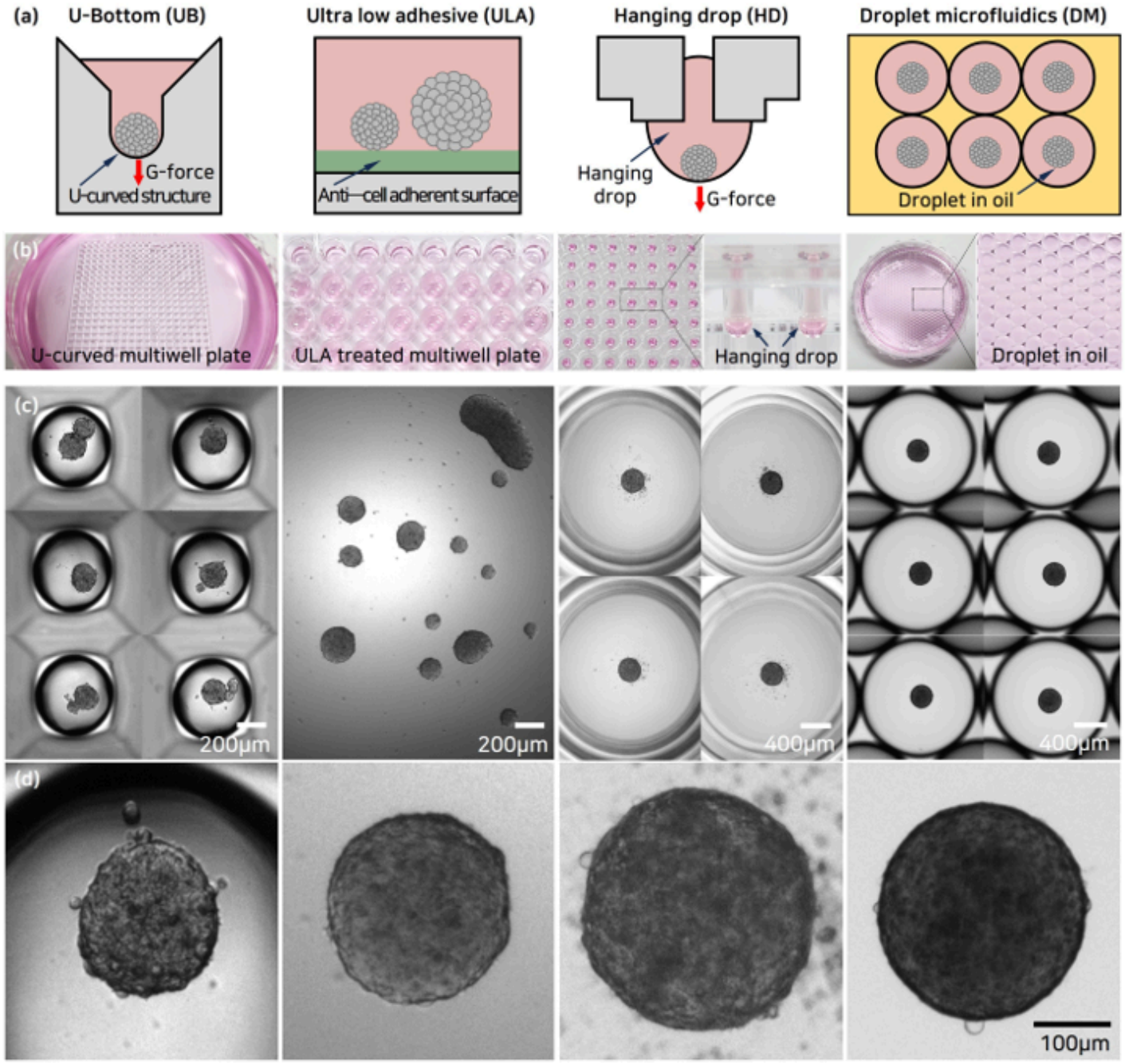


Figure 2

(a) Detailed schematics and (b) optical images of the four platforms used in this study. (c) As-fabricated MTS from each platform before collection, and (d) high magnification microscopic image.

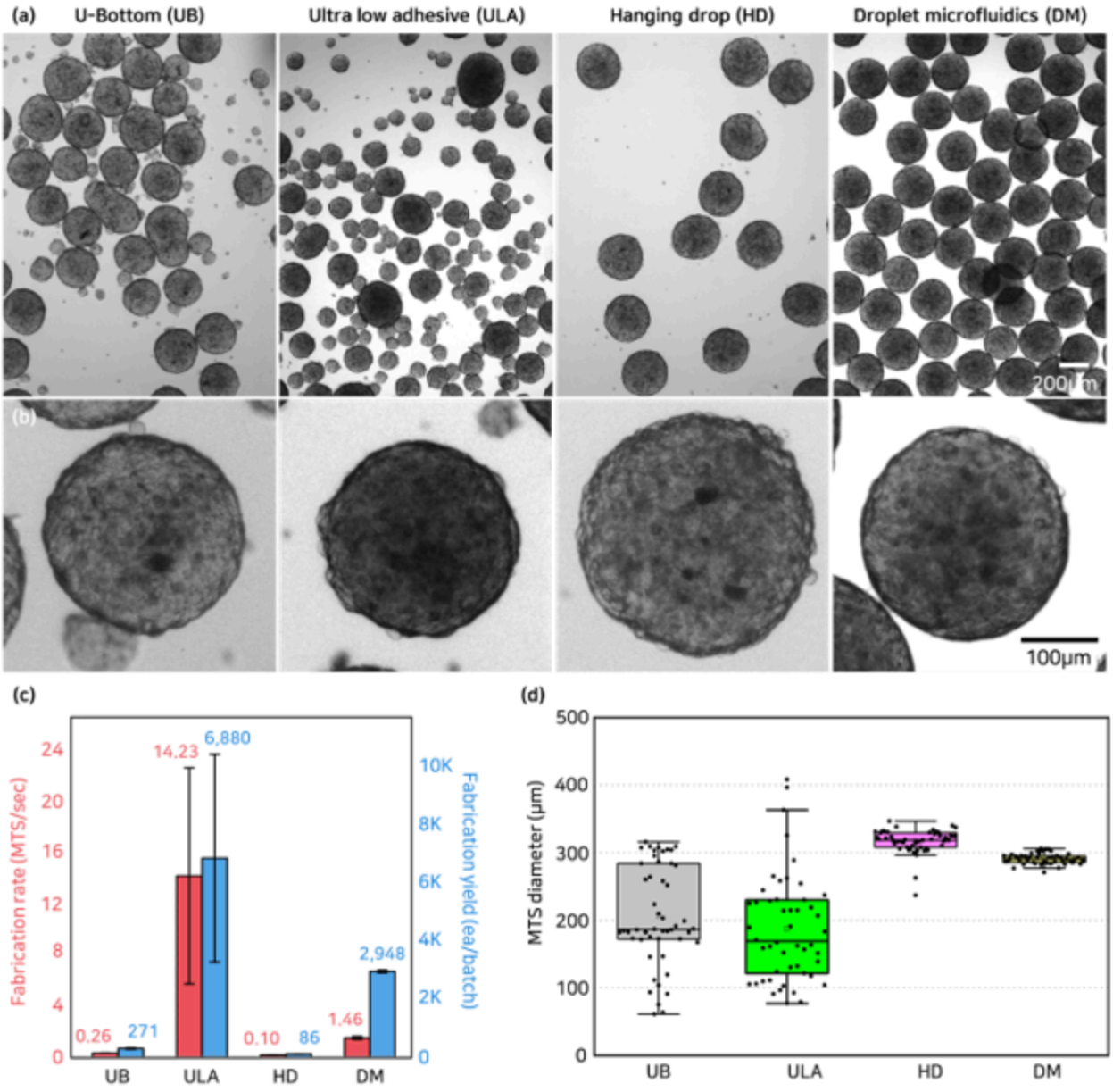


Figure 3

(a) Collected MTS from each platform, and (b) high-magnification microscopic image. (c) The number of MTS fabricated per second in each platform and the yield of MTS fabricated per batch. (d) Size distribution of MTS with a target diameter of 300 μm on each platform.

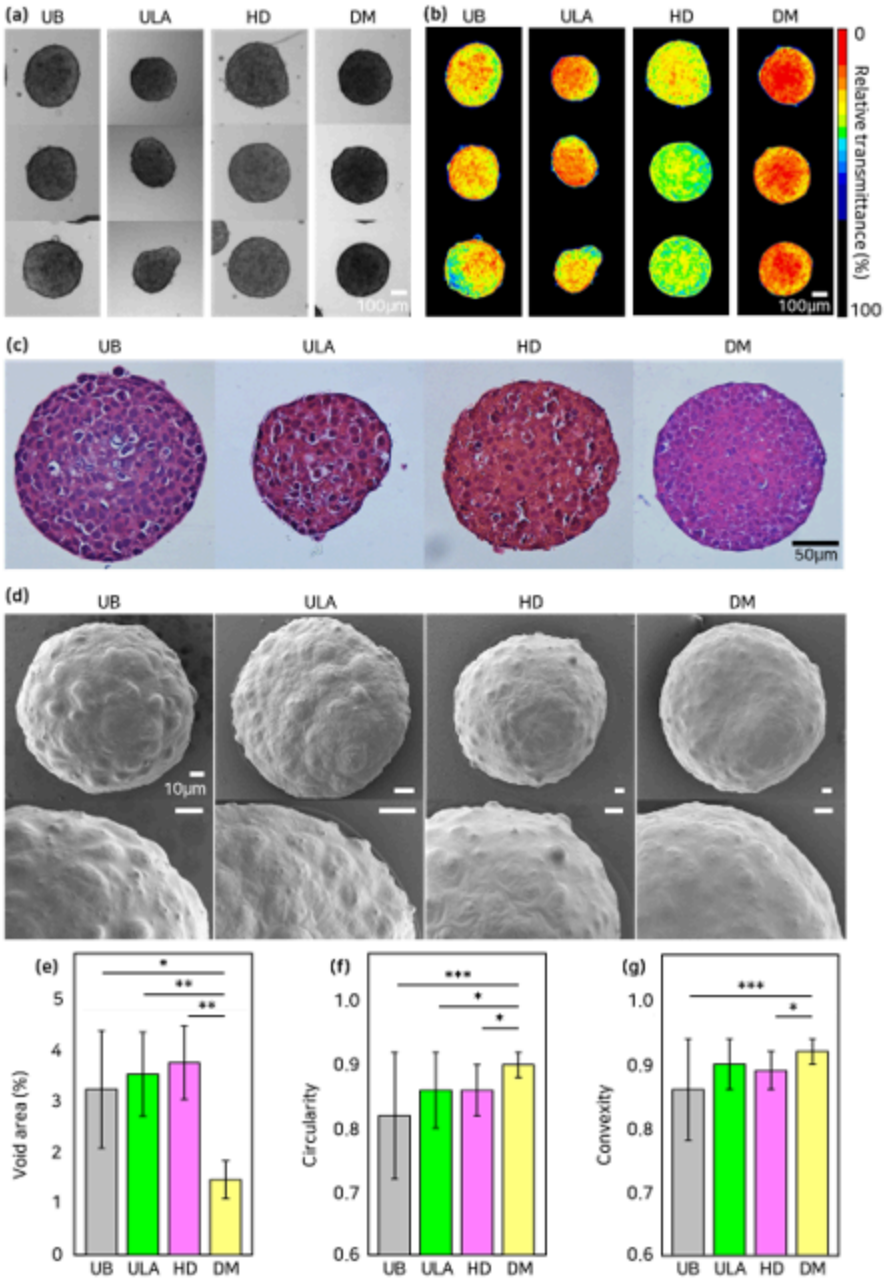


Figure 4

(a) Brightfield microscopic images of MTS, (b) heatmap images converted from brightfield images based on transmittance, and (c) cross-sections of MTS from each fabrication platform to assess compactness. (d) SEM images showing surface morphology of MTS, (e) void areas measured in MTS cross-sections, (f) quantitative graph of circularity, and (g) convexity. Statistical significance was defined as $p < 0.05$ (*), $p < 0.01$ (**), and $p < 0.001$ (***).

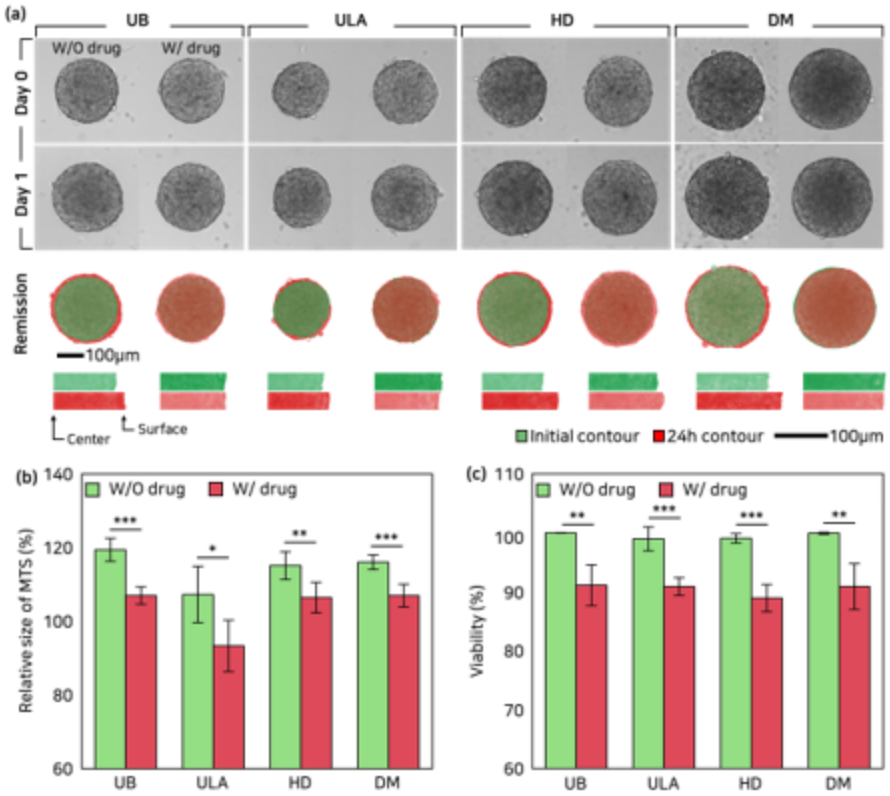


Figure 5

(a) The drug-induced remission of MTS fabricated for each platform, and with and without the drug. (b) The relative size change and (c) cell viability within MTS according to the fabrication platforms. Statistical significance was defined as $p < 0.05$ (*), $p < 0.01$ (**), and $p < 0.001$ (***).

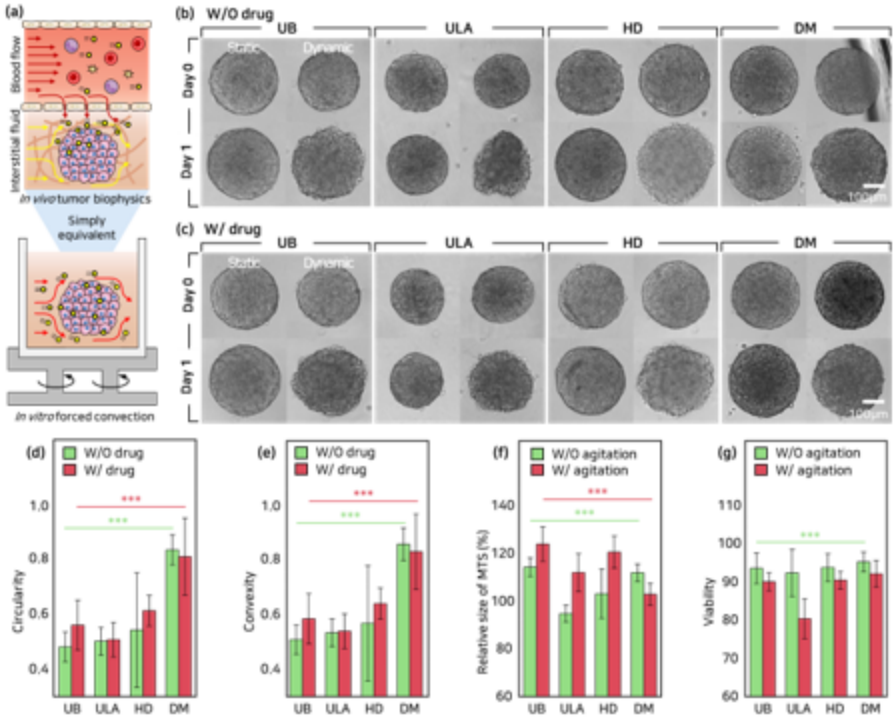


Figure 6

(a) Schematic for mimicking the *in vivo*environments with agitation. (b) MTS in static and dynamic states without the drug and (c) with the drug. (d) Circularity and (e) convexity of MTS fabricated from each platform in dynamic states. (f) Relative size of MTS according to each platform. (g) Cell viability under dynamic states. Statistical significance was defined as $p < 0.05$ (*), $p < 0.01$ (**), and $p < 0.001$ (***).

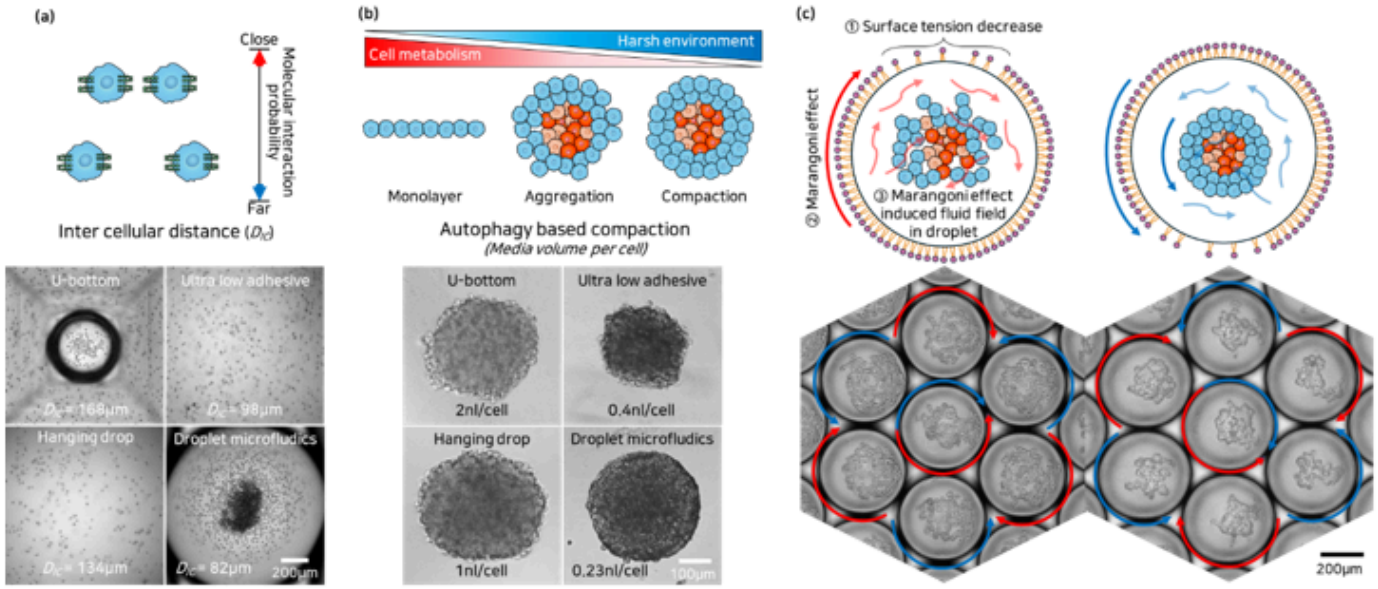


Figure 7

(a) A schematic where intercellular distance affects molecular interactions (top), and the intercellular distance immediately after cells were seeded on each platform (bottom). (b) A schematic where MTS compaction and the limited nutrients may affect MTS formation (top), and the volume of media available per cell on each platform (bottom). (c) Fluid flow induced by the Marangoni effect acting on the droplet promote MTS formation.

Supplementary Files

This is a list of supplementary files associated with this preprint. Click to download.

- RevisedSupportinginformation.docx